Non-intrusive characterization of particle size changes in fluidized beds using recurrence plots

Savari, Chiya; Sotudeh-Gharebagh, Rahmat; Zarghami, Reza; Mostoufi, Navid

DOI:
10.1002/aic.15265

License:
Other (please specify with Rights Statement)

Document Version
Peer reviewed version

Citation for published version (Harvard):
Savari, C, Sotudeh-Gharebagh, R, Zarghami, R & Mostoufi, N 2016, 'Non-intrusive characterization of particle size changes in fluidized beds using recurrence plots', *AIChE Journal*, vol. 62, no. 10, pp. 3547-3561. https://doi.org/10.1002/aic.15265

AIChE Journal
DOI 10.1002/aic.15265

Non-Intrusive Characterization of Particle Size Changes in Fluidized Beds Using Recurrence Plots

Chiya Savari, Rahmat Sotudeh-Gharebagh*, Reza Zarghami, Navid Mostoufi

School of Chemical Engineering, College of Engineering, University of Tehran, Tehran, 11155/4563, Iran

Abstract

An on-line method is developed for monitoring of mean particle size in fluidized beds using pressure fluctuations (PF) and acoustic emissions (AE) signal by recurrence plot (RP) and recurrence quantification analysis (RQA). PFs and AE signals of a lab-scale fluidized bed were measured simultaneously at various superficial gas velocities and mean particle sizes. Although the AE signals are often very complicated due to many different acoustic sources in the bed, applying RP analyses showed that small changes in mean particle size can be detected by visual comparison of AE-RP structures, while this cannot be distinguished by graphical RP analysis of PFs. Moreover, the hydrodynamics of the bed was inspected through RQA analysis of both signals. For this purpose, recurrence rate, determinism, laminarity, average length of diagonal and vertical lines were extracted from RPs showing the effect of an increase in the mean particle size.

Keywords: fluidized bed, particle size, pressure fluctuations, acoustic emissions, recurrence plot

* Corresponding author, Tel.: (+98-21)6696-7797, Fax: (+98-21)6696-7781, E mail: sotudeh@ut.ac.ir

Received: Sep 03, 2015; Revised: Feb 02, 2016; Accepted: Mar 28, 2016

Introduction

Fluidization is a process in which solid particles are suspended in a gas or liquid phase and become fluidized, similar to the state of a liquid. Gas-solid fluidized beds are widely used in physical and chemical processes, such as agricultural, food, metallurgical, environmental and pharmaceutical. Some advantages of this process are efficient contact between fluid and particles, thermal homogeneity, high mixing and high heat and mass transfer rates as compared to conventional processes.[1-5] In spite of these advantages, this process has a number of disadvantages limiting its industrial applications. Hydrodynamics of a fluidized bed may be altered over time due to either imposed or unwanted changes in superficial gas velocity and mean particle size which may result in partial or complete defluidization of the bed. Various researchers have reported the defluidization to happen during gasification or combustion of coal, waste or biomass[6-8] as well as coating and granulation of particles.[9-11] Conditional monitoring of gas-solid fluidized beds is important since the performance of these beds strongly depends on its hydrodynamics.[12-14] A method capable of observing small changes in the hydrodynamics of fluidized bed is not only useful for preventing undesirable situations (e.g., agglomeration and defluidization), but also it is applicable to the control of product quality, both in batch and continuous operations.

Many techniques have been developed for characterization of the hydrodynamics, detection of agglomeration and identification of the onset of defluidization. These techniques are based on the measurement of various parameters, such as pressure fluctuations (PFs), temperature, acoustic emissions (AE), voidage and vibration signature.[8,15-18] PFs are easily measurable reflecting the effect of different hydrodynamic properties of the bed such as gas turbulence and bubble passage, coalescence and eruption. Therefore, this measurement technique

was applied in this work for monitoring of small changes in fluidized bed hydrodynamics. The main uncertainty accompanied with the pressure measurement is that the pressure transducer may disrupt the flow of gas and particles. Moreover, application of the pressure measurement has some limitations under severe, corrosive and high pressure/temperature conditions.[16] Consequently, several non-intrusive techniques have been developed to address these main limitations and avoid the probe interference problem.[16] In the non-intrusive methods, the measuring probe is placed out of the bed, thus, the hydrodynamics of the bed is not affected by the probe. Also, these methods can be used in severe operational conditions.

Measurement of acoustic emissions, as a non-intrusive measurement technique, has shown a potential to increase process understanding and to provide a basis for on-line monitoring and control of fluidized beds.[19-23] Analysis of AE signals is applicable to a wide range of process conditions, is of low cost and is a reliable technique in the process being monitored. In the AE measurement technique, direct contact of the measuring probe with the bed is not required; allowing real-time, on-line monitoring with little or no intrusion. Also, the AE signals contain information from particle-particle and particle-wall collisions, as well as of the motion of the bubbles. As such, it is suitable for characterizing the fluidized bed dynamics. Tsujimoto et al.[23] calibrated an AE sensor for fluidized bed granulation of microcrystalline cellulose spheres of uniform size at various operating conditions. Their results led to development of a method for detecting the onset of unstable fluidization conditions. Briongos et al.[20] identified different flow regimes in a fluidized-bed granulator using glass ballotini beads by applying time, frequency and state space analysis of AE signals. Briens et al.[19] demonstrated the potential of this technique in a high-shear granulation for end-point detection using mean frequency of AE signals. Hansuld et al.[21] showed audible acoustic emissions can be used to monitor and detect end-point of

granulation. In addition, Gamble et al.[22] developed a multivariate model for detecting the end-point in a small-scale granulator using AE.

Many researchers have investigated fluidized bed hydrodynamics by analysis of different signals in time, frequency and state space domains. Time domain analysis typically includes the analysis of statistical properties of the measured signal such as, standard deviation, skewness and kurtosis.[12,24] Fast Fourier and wavelet transforms have been extensively used for analysis of fluidized beds in frequency domain.[25,26] However, the hydrodynamics of gas-solid fluidized beds are governed by complex nonlinear dynamic relationships and a proper understanding of the state of a fluidized bed cannot be determined by linear methods in time and frequency domains. Various nonlinear analysis methods, such as short-term predictability[8] and attractor comparison in the state space have been used for analyzing the dynamic changes in the fluidization hydrodynamics.[7, 27] All methods of nonlinear time series analysis are based on construction of an attractor of the dynamic evolution of the system in the state space.

Although, nonlinear analysis can give a better understanding of the system state, however these methods are accompanied with some drawbacks and limitations such as, long term data sampling, time consuming numerical calculations and uncertainty in the determination of embedding parameters.[14] In other words, different reconstruction methods can lead to different embedding dimensions.[14] In this study, monitoring techniques based on the recurrence plot (RP) and recurrence quantification analysis (RQA) of PF and AE signals are developed for the detection of small changes in particle size during fluidization. Recurrences in the dynamics of a fluidized bed can be visualized by the RP which has been introduced by Eckmann et al.[28] The main feature of the RP is that a high-dimensional dynamical system, whose state space trajectory is difficult to visualize, can be represented in a two-dimensional plot. Another considerable

characteristic of the RP analysis is that it gives useful information using a small amount of data points. In other words, the problems associated with typical nonlinear analysis methods, such as long-term data samplings and time consuming algorithms, can be solved when RP method is used.[29-32] This work focuses on developing a methodology for detecting small changes in mean particle size based on PF and AE monitoring in a gas-solid fluidized bed. For this purpose, the RP structures and different RQA parameters (recurrence rate, determinism, laminarity, average diagonal length and trapping time) of both pressure fluctuations and acoustic emission signals were obtained and analyzed at different particle sizes.

Experiments

The column was made of Plexiglas with 15 cm in inner diameter and 2 m in height. Compressed air at ambient conditions (1 atm, 25 ºC) was entered into the column through a perforated plate distributor with 435 holes of 7 mm arranged in a triangular pitch. A cyclone was used to separate fine particles from air at high superficial gas velocities and return them back into the bed. A pressure regulator and dehumidifier were used in the air supply line to eliminate possible fluctuations and to provide air at constant pressure (8 bars) and humidity. Sand particles (Geldart B) with mean sizes of 368 μm (type I) and 835 μm (type II) and particle density of 2350 kg/m^3 were used in the experiments. The experiments were carried out at superficial gas velocities ranging from 0.1 to 0.6 m/s. In order to investigate the sensitivity of the method to changes in the mean particle size, each experiment was started out with only sand type I in the bed and then substituting 5%, 10% and 15% of the bed particles with sand type II. This corresponds to an average particle size increase from 368 μm to 378, 390 and 402 μm,

respectively. Total mas and static height of the bed were constant in all experiments and the aspect ratio of the bed was set to 1.5 (L/D=1.5).

Absolute pressure fluctuations were measured by a pressure probe (Kobold, SEN-3248) which was screwed onto the bed wall at 15 cm above the distributor. This probe had a response time of less than 1 ms and a fine mesh net was used on its tip for avoiding the blockage of the probe. Measured PFs were band-pass filtered at lower cut-off frequency of 0.1 Hz and upper cut-off frequency of 200 Hz (Nyquist frequency). The filtered signals were then amplified and sent to a 16 bit data acquisition board (Advantech 1712L). The sampling frequency of 400 Hz was used in this work based on recommendation of Johansson et al.[33] and van der Stappen et al.[34] that suggested the sampling frequency should be in the range of 5-100 times the average cycle frequency (typically between 100 and 600 Hz). The PFs were measured for 200 s which corresponds to 80,000 data points.

The AE sensor was glued externally to the outer surface of the bed at 15 cm above the distributor. The AE signals were measured by an omnidirectional back electret condenser microphone (Panasonic, WM-61 A) which had a frequency response of 20-20000 Hz (sensitivity -35±4 dB, signal to noise ratio more than 62 dB). The outlet signal from the microphone was recorded by a USB interface sound analyzer (ARTIMAN Instruments, ART-SA16) for 60 s with a sampling frequency of 44 kHz. This frequency was determined using the Shannon-Nyquist criterion which states that the sampling frequency should be at least twice the maximum frequency of the signal.[24] For this purpose, the power spectral density functions of the AE signals at various sampling frequencies were calculated and it was concluded that there is no dominant frequency greater than 10 kHz in the signal. Thus, the AE signals were recorded at the sampling frequency of 44 kHz to avoid the risk of alias according to the Shannon's theorem.

Theory

Recurrence plot, introduced by Eckmann et al.,[28] visualizes recurrences in the dynamics of a dynamical system. The RP represents the times at which states of a phase space of the system is repeated. Although the attractor reconstruction in a state space depends on the embedding dimension, the RP, however, may be constructed without embedding.[35] While high-dimensional state space trajectories are very difficult to visualize, any state space trajectory can be represented in a two-dimensional plot by the RP.[28,36] Moreover, short-term data can be used to visualize the dynamics of a system by a RP and this feature eliminates the need for time consuming long-term data.[37] These features make the RP a very potent tool to study the hydrodynamics of fluidized beds.

Definition of RP

The RP is a two-dimensional squared matrix, R, which is mathematically expressed as:

$$R_{i,j} = \Theta\left(\varepsilon - \left\|\vec{x}_i - \vec{x}_j\right\|\right) \quad i,j = 1,2,3,\dots,N \tag{1}$$

where N is the number of state space points, $\vec{x}_i$, $\vec{x}_j \in R^m$ are i-th and j-th points of the m-dimensional state space trajectory, ε is a threshold distance, $\|.\|$ is the norm and $\Theta(.)$ is the Heaviside function. In fact, the matrix R compares the states of the system at times i and j. If the states are similar (norm is less than ε), this would be indicated by a one in the matrix, i.e., $R_{i,j}$=1, and a black spot would appear on the plot at coordinate (i, j). If, on the other hand, $\vec{x}_i$ and $\vec{x}_j$ are rather different (norm is greater than ε), the corresponding entry in the matrix would be $R_{i,j}$=0 and a white spot would appear on the plot.

Construction and structures of RP

Construction of the RP starts with a measured time series of the system:

$$x_i = \{x_1, x_2, x_3, \dots, x_N\} \quad (2)$$

Then, the attractor of the state space is reconstructed from this time series.[38] In this reconstruction, elements of the time series become coordinates of the *m*-dimensional space:

$$\overrightarrow{x_i} = \sum_{k=1}^{d} x_{[i+(k-1)\tau]} . \overrightarrow{e_k} \quad i = 1,2, \dots, M, \;\; M = N - (m-1)\tau \quad (3)$$

where $\vec{x}_i$ is the state space trajectory of the time series, *m* is the embedding dimension of the state space, τ is the time delay vector and $\overrightarrow{e_k}$ is the unit vector of the axis. Next, the distance matrix (DM, $D_{i,j}=(\vec{x}_i, \vec{x}_j)$) between the reconstructed points in the trajectory of the state space are computed. Here, $D_{i,j}$ is a certain type of distance applied to the trajectory, such as Euclidean norm, maximum norm, normalized norm, etc.[37] The DM is an array of distances in an $M \times M$ matrix, where *M* is the number of state space vectors. The DM matrix is converted to the recurrence matrix using the radius threshold. Each element of the DM which is smaller than ε is considered as a recurrence point and forms a black spot; otherwise it forms a white spot in the recurrence matrix. Figure 1 represents the reconstruction of RP graphically.

Black and white points in a RP form various geometric structures which are related to the behavior of dynamical system. These structures in the RP consist of two different local patterns: local white areas (LWA) or bands and local bold areas (LBA). The LWA, or white patches, represent the points which fluctuate with relatively high amplitude in the signals. These are points on peaks of the signal and points that their values are about the mean value of the signal. In these points, the distance between points of the state space trajectory is longer than the radius threshold. Therefore, these are not considered as recurrence points. In contrast, black patches, or LBA, correspond to times when the signal does not strongly fluctuate.

Patterns in a RP reflect the dynamics of the system under consideration. In a fluidized bed, patterns in the RP obtained from the bed during its operation include much useful information about its hydrodynamics. Zarghami et al.[14] used PFs to study the hydrodynamics of the fluidized bed and concluded that PFs represent interaction of three different phenomena in a fluidized bed: large PFs of low frequency correspond to macro structures (large bubble eruptions and movement of larger bubbles), meso structures of higher frequency dynamics of clusters of dense phase and small bubbles and micro structures of very high frequencies which represents interaction among single particles and fluid as well as noise. Therefore, LWAs in RPs are related to macro phenomena (e.g., bubble eruption, bubble generation and large bubble movement) and LBAs represent finer structures (e.g., clusters, particle interaction). Thus, the RP can help to visually identify the dynamics of the fluidized bed.[29-32]

Recurrence quantification analysis

Several methods have been proposed for measuring the complexity of structures in a RP.[37,39-41] These methods quantify small-scale structures of RPs and are known as recurrence quantification analysis (RQA). The RQA involves estimation of recurrence point density and diagonal and vertical lines in a RP. Patterns within a RP (and subsequently the RQA parameters) are related to different dynamics of the system. Hence, valuable information about the dynamics can be extracted from the RP patterns and RQA analysis. Among various RQA parameters, recurrence rate, determinism, laminarity, average diagonal line length and trapping time were used in this study. Also, in order to investigate the sensitivity of the RP and RQA method to changes in the particle size, the time series were first normalized as followings:

$$x_{i,n} = \frac{x_i - \bar{x}}{\sigma_x} \quad (4)$$

This normalization reduces the sensitivity of the method to small changes in the superficial gas velocity.[7,32]

Recurrence rate (RR), or per cent recurrence, is the simplest measure in the RQA which represents the density of recurrence points in the RP and is defined as:

$$RR = \frac{1}{N^2} \sum_{i,j=1}^{N} R_{i,j} \quad (5)$$

where $\sum R_{i,j}$ is the total number of repeated points while N^2 is the total number of points in the recurrence matric. Hence, the RR measures the fraction of recurrence states which have happened in the time series.

Determinism (DET) is the ratio of recurrence points that form diagonal structures (of at least length l_{min}) to all recurrence points and is defined as:

$$DET = \frac{\sum_{l=l_{min}}^{N} lP(l)}{\sum_{l=1}^{N} lP(l)} \quad (6)$$

where $P(l)$ is the number of lines with the length of l, $\sum lP(l)$ is number of block dots forming the diagonal lines and l_{min} is minimal length of diagonal lines. Determinism measures the predictability (rule-obeying) of the system and is low for a stochastic system and high for a periodic system.[37,42] Therefore, it can be said that the determinism measures the probability of similar changes in the RP.

Similar to the definition of determinism, the ratio of recurrence points forming vertical lines with length v to all recurrence points can be computed and is called laminarity (LAM):

$$LAM = \frac{\sum_{v=v_{min}}^{N} vP(v)}{\sum_{v=1}^{N} vP(v)} \quad (7)$$

where $P(\nu)$ shows the number of lines with the length of ν, $\sum \nu P(\nu)$ represents the number of dots forming the vertical lines and ν_{min} is minimal length of vertical lines. The laminarity shows probability occurrence of states which do not change or change very slowly (laminar states), so laminarity corresponds to the amount of laminar states in the system. Usually, ν_{min}=2 is an appropriate value for evaluating the laminarity.[37]

Among RP structures, a diagonal line with length l means that a part of the state trajectory is rather close to another part of the trajectory for l time steps. In other words, the distance between parts of a state trajectory is shorter than the threshold distance and the trajectory stays within an ε-distance around another segment of the trajectory for l time steps. From this point of view, average diagonal line length (L_{mean}) can be introduced as another RQA parameter which is related to the average time that two segments of the trajectory visit the same regions (consequently the system visit the same dynamical states) and can be interpreted as the time during when the system has the same dynamical states (mean prediction time). The average diagonal line length is mathematically defined as:

$$L_{mean} = \frac{\sum_{l=l_{min}}^{N} lP(l)}{\sum_{l=l_{min}}^{N} P(l)} \quad (8)$$

The last RQA parameter introduced here is the average length of vertical lines which is called trapping time (TT) and represents the mean time that the system stays in a specific state (or how long the state is trapped). The minimal length ν_{min} is need for calculation of TT, as in the case of LAM. The trapping time is defined as:

$$TT = \frac{\sum_{\nu=\nu_{min}}^{N} \nu P(\nu)}{\sum_{\nu=\nu_{min}}^{N} P(\nu)} \quad (9)$$

Results and Discussion

Setting of input parameters

Input parameters of RP and RQA methods (m, τ, ε, l_{min} and υ_{min}) should be carefully determined before plotting RPs and evaluating RQA parameters. The epoch length of time series (L) is selected in such a way that RQA parameters remain constant when more than L data points are used. Figure 2 shows the evolution of RR and DET of PFs and AE signals with the number of data points. The figure shows that these parameters (as well as other RQA parameters, not shown here) become invariant against the number of data points when a large enough number of data are used (3000 for PFs and 5000 for AE signal). Therefore, in the following, 3000 (7.5 sec.) and 5000 (114 msec.) data points were used for evaluating RQA parameters of PFs and AE signals, respectively. Tahmasebpour et al.[43] and Sedighikamal and Zarghami[44] also used short term data to analyze RPs of fluidization PFs.

The embedding dimension (m) is the next recurrence parameter to be fixed. Figures 3 and 4 show RPs of PFs and AE signals of the fluidized bed, respectively, at 0.2 m/s superficial gas velocity with four different embedding dimensions. As seen in these figures, qualitative features of the four RPs are essentially the same. The major difference between these figures is the gradual fading of RP as m is increased. This is due to the fact that an identical radius threshold (ε) was used for each plot. Therefore, it can be concluded that the general nature of RP structures are independent of the embedding dimension. The same results were reported by Iwanski and Bradley,[45] Thiel and Romano[46] and March et al.[35]

For investigating the effect of the embedding dimension on RQA parameters, determinism and laminarity of PFs and AE signals were calculated at different embedding dimensions. For this purpose, the same value for RR was set and then DET and LAM were computed at various embedding dimensions. Constant RR provides the same number of black

points in each of RP. Variations of DET and LAM of PFs and AE signals at superficial gas velocity of 0.2 m/s and different fractions of sand type II in sand type I are shown in Figure 5. According to this figure, values of DET and LAM just shifted to higher values by increasing m, while the trend of parameter variations versus the change of average particle size is preserved. It should be mentioned that the same effect was been observed for other RQA parameters (L_{mean} and TT, not shown here). Therefore, it can be concluded that the same results can be obtained in RQA with no embedding and the embedding dimension can be set to 1 to make calculations easier. This is an important advantage of RPs compared to other techniques of nonlinear data analysis.

Time delay (τ) is the next input parameter and should be selected such that to minimize the mutual information function of the time series.[47] For this purpose, RPs and RQA parameters of PF and AE signals were obtained at different time delays and it was found that they are not sensitive to the value of time delay. This is advantageous in characterizing the fluidized bed hydrodynamics based on RQA method since it is not necessary to find the optimum time delay. Most researchers[32,43,44] also found that time delay is a non-critical parameter and most systems are rebuts and stable against changes in this parameter.

The third input parameter is the radius threshold (ε) which determines the number of points to be appeared in the RP. The proper value of ε depends on the process and its operating conditions. However, in general, it is desirable to choose the smallest value as possible. In this study, similar to literature,[29-32] this parameter was selected based on three guidelines proposed by Webber and Zbilut:[41] (i) the radius threshold should fall within the linear scaling region of the RR vs. ε in a full logarithmic plot; (ii) RR must be kept low (e.g., 0.1% to 5%); and (iii) the DET should not be saturated (to be 100%) at selected ε. Figures 6a-b show RR and DET versus radius

threshold for PFs and AE signals, respectively. It can be seen from these figures that the value of 0.05 satisfies all mentioned guidelines. Also, the value of ε was set the same for PF and AE signals to compare the results at the same values of input parameters.

A typical value for the minimal length of diagonal and vertical lines (l_{min} and v_{min}) is 2.[31,32,48] Babaei et al.[48] analyzed determinism of the Lorenz system and found that the proper value of l_{min} is 2 and used this value for investigating the hydrodynamic of fluidized beds. Therefore, the minimal length of vertical and diagonal lines was considered to be 2 in this work. Optimum values of input parameters for both PFs and AE signals are given in Table 1. Moreover, it should be noted that for RQA calculations, the original signal partitioned into smaller windows or epochs (L=3000 points for PFs and L=5000 points for AE signal). Adjacent windows were offset by 1500 points (50% overlap) and 3750 points (25% overlap) for pressure and acoustic time series, respectively. Recurrence quantification parameters were then computed for each sliding windows over the total time series (200 sec for PF and 60 sec for AE signal) and the average value has been reported as the RQA parameter.

Sensitivity to particle size changes

Figures 7a-d show the RP of PFs at superficial gas velocity of 0.2 m/s at different fractions of sand type II in sand type I. As mentioned above, these fractions correspond to average particle sizes of 368 μm to 378 μm, 390 μm and 402 μm, respectively. It can be seen in these figures that there are many recurrence points with clear regular patterns, indicating the periodic behavior of PFs. The recurrence points forming diagonal and horizontal lines suggest that special structures exist in RP of PFs which reflects different phenomena taking place in the bed, such as bubbles formation as well as their coalescence and eruption. It can be seen in Figure

7 that structures in RP of pressure fluctuations differ when the fraction of sand type II in sand type I is changed. Nevertheless, changes in the fraction of LBA and LWA are not clearly visible. Thus, visual observation of the graphical display of RP of PFs is insufficient for an observer to discriminate and interpret the effect of particle size on patterns presented within the RP. This shortcoming reveals the need for procedures to quantify RP structures.

Figures 8a-d represent the RP of AE signals at superficial gas velocity of 0.2 m/s and different fractions of sand type II in sand type I. It can be seen in these figures that the size of LWAs increases with increasing the fraction of sand type II. This trend shows that the amplitude of AE signals becomes higher when increasing the average particle size. In contrast to RPs of PFs, changes in the size of LWA within RPs of AE signals are obvious even without any quantification analysis. This reveals that the large scale appearance and typology of RPs of AE signals can easily be used to estimate the changes in the average particle size in fluidized beds. These observations show that PFs and AE signals reflect different characteristics of fluidization hydrodynamics based on different physical mechanisms. PFs in a fluidized bed are related to the following phenomena which can be attributed to three different structures: eruption and movement of large bubbles (macro structure), movement of clusters of dense phase and small bubbles (meso structure) and movement of single particles (micro structure). Macro and meso structures are dominant structure represented in pressure fluctuations.[14] Small changes in average particle size of the bed do not result in regime transition and therefore, a vast variation does not occur in the macro structure of the bed (e.g., bubble eruption, bubble generation and bubble coalescence).[49] Subsequently, appearance of the RP obtained by PFs does not show a considerable change when particles size is changed to some extent.

He et al.[50] showed that the AE signal in a gas-solid fluidized bed mainly originates from collisions between particles and the wall, which mainly represents the behavior of micro-structure (i.e., interactions among particles and between particles and fluid). Thus, the main differences between AE signals and PFs can be summarized as: (i) most of the information in PFs comes from macro and meso structures in the original signal and they mainly represent the dynamic interactions between solids and bubbles; (ii) the main information in AE signals arise from micro structures and the original AE signals illustrate mainly the dynamics of particle motion in a fluidized bed. Hence, it can be recommended to use PFs measurement for characterization of bubble-related properties (e.g., bubble size, bubble velocity, wake vortex, etc.). In contrast, the AE measurement technique is more suitable for characterization of particle-related properties (e.g., average particle size, particle size distribution and particle density).

Figures 9a-d and 10a-d illustrate RPs of PFs and AE signals, respectively, at superficial gas velocity of 0.6 m/s and different fractions of sand type II in sand type I. Similar to Figures 7a-d and 8a-d, the size of LWAs in the RPs increases with increasing the fraction of sand type II (larger particle size), but the changes are more visible in the RPs of AE signals. Increase in the average particle size affects the bed hydrodynamics by increasing the minimum fluidization velocity (U_{mf}) and velocity of onset of turbulent fluidization (U_c). These values for sand type I and mixtures of the two sand types used in this work are given in Table 2. Therefore, it can be seen that in all experiments of this work that the fluidized bed was operating at the bubbling regime. Babaei et al.[32] and Tahmasebpour et al.[30] demonstrated that the RP structures of PFs are almost insensitive to minor variations in the superficial gas velocity as long as there is no change in the fluidization regime. This can also be observed in this work by comparing the corresponding RPs of PFs in the different gas velocity in the bubbling regime (Figures 7a-d and

Figures 9a-d). However, it can also be seen from Figures 8a-d and 10a-d that the fraction of LWAs in RPs of AE signals increases with increasing the gas velocity from 0.2 to 0.6 m/s. This increase in LWAs can be related to the enhancement of solid mixing which produces AE signals with higher amplitude at higher gas velocities. Note that a signal with higher amplitude has a lower recurrent states or black dots. Babaei et al.[32] also concluded that at higher gas velocities, RPs and RQA parameters of PFs become less sensitive to changes in the particle size. However, it can be seen in Figures 8a-d and 10a-d that patterns of RPs obtained by AE signals are more sensitive to changes of particle size at higher gas velocity. In fact, variation in size of LWAs of AE-RPs in Figures 10a-d is more visible than that in Figures 8a-d. This suggests that analyzing the AE signals is an effective tool to characterize the particle-related properties and mixing at high gas velocities in gas-solid fluidized beds.

As previously mentioned, overall patterns in a RP and their typology can provide some useful insight in the dynamics of the dynamical system. However, detecting changes of finer patterns need quantitative analysis. In this study, the graphical display of the RP is further quantified by RQA in terms of RR, %DET, %LAM, L_{mean} and TT. For this purpose, values of these RQA parameters as a function of average particle size for two superficial gas velocities are shown in Figures. 11-13 and are discussed below. It should be noted that the 95% confidence interval was calculated for each RQA parameter.[51] These confidence intervals are shown by error bars in Figures 11-13.

Figures 11 illustrate variations of RR of PFs and AE signal, respectively, against average particle size. This figure shows that the RR for both PFs and AE signal decrease with increasing the average particle size. The RR simply counts the black dots in the RP, excluding points on the main diagonal line (since $R_{i,i}$=1 for any i) and measures the relative density of recurrence points

in the RP. As mentioned previously, there is no visible change in the graphical display of RPs of PFs when increasing the average particle size. Nevertheless, the trend of recurrence rate, shown in Figure 11, illustrates that the relative density of black dots decreases with increasing the particle size which can be related to increase in the contribution of macro-scale structures (i.e., increase in size of bubbles). Since larger particles are added to the bed in each step, number of bubbles decreases but they grow in size. The amplitude of PFs is proportional to the size of bubbles[14] and larger bubbles produce PFs with higher amplitude. The recurrent states, or black points, are less in larger amplitude PFs. This is the reason that a smaller RR is observed for PFs when the average particle size is increased. Nevertheless, this increase in the contribution of bubbles is not high enough to be detected in the graphical display of pressure RPs. The same trend can be observed in the RR of AE signals against particle size, shown in Figure 11, with the difference that it is more sensitive to changes in the particle size. Larger particle collisions produce AE signals with higher energy. Therefore, the corresponding AE signals become of higher amplitudes. This can be attributed to the sound of particles when splashing on the bed surface due to bubbles bursting. Thus, smaller RR is observed in the presence of larger particles. The higher sensitivity of RPs of AE signals can be validated by comparing variations of RR values versus particle size for both PFs and AE signals in Figure 11.

Figure 12a shows the determinism variations for both PFs and AE signals when the average particle size is increased. The trend of determinism is contrary to recurrence rate and it increases with increasing the average particle size at a constant gas velocity. Increase in the determinism indicates that the behavior of the bed has become more periodic and predictable. As larger particles are added to the bed, the minimum fluidization velocity increases and bubbles start to fall in number and grow in size. Behavior of larger bubbles is more predictable than

smaller ones, hence, the bed behavior becomes more predictable and PFs approach that of a periodic time series. Thus, RP plots of PFs at the presence of the larger particles have higher determinism.

The bubble movement is responsible for internal solid circulation in gas-solid fluidized beds.[1,52] Wang et al.[52] showed that there are many small flow circulation cells across the bed above the distributer. Also, the emulsion solids circulate as vortex ring above these small flow cells, named main fluidization zone, that have more stable fluidization conditions. When bubbles proceed up through the bed, there is exchange of material between the wake and the surrounding bulk. The solid particles are splashed onto the surface of the bed and return back to the underside along the wall as the bubble reaches the top. There are also stagnant zones between the main fluidization zone and the small circulation cells above the distributor. Wang et al.[52] indicated that in stagnant zones, particles are less active compared to the main fluidization zone. Stagnant zones in the bed increase when the bed was fluidized with larger particles. Also, the total number of particles in the bed decrease by adding larger particles at the same mass of particles. This means that less of particles take part in generation of AE signals when larger particles are added to bed. The AE signal generated by less number and larger particles in a fluidized bed is more periodic and predictable. Therefore, the determinism of AE signals increases with increasing the average particle size.

According to Figure 12b, variation of laminarity against particle size of both PFs and AE signals is similar to determinism. As mentioned earlier, laminarity reflects the probability occurrence of a specific state that does not change or change slowly while determinism measures the probability occurrence of similar states in the RP. As can be seen in Figure 12b, laminarity of both PFs and AE signals increases with increasing the particle size. As pointed out before, the

portion of macro structures (large bubbles) increases in a bed of larger particles and the PFs exhibit a more periodic behavior. This is in agreement with the interpretation of laminarity which is related to the amount of laminar states. On the other hand, finer structures, like motion of particles, small bubbles and clusters, show more turbulent behavior and consequently their laminarity are low. Increase in the average particle size affects the bed hydrodynamics by increasing the minimum fluidization velocity (U_{mf}). At a constant superficial gas velocity, the fluidization quality and particle velocity decreases as larger particles added into the bed. The reduction in the particle velocity and number of particle collisions results in producing AE signals with a higher laminar state. Hence, laminar structures (which correspond to bubble movement in the case of PFs and particle motion with lower velocity in the case of AE signals) would happen more frequently in a bed of larger particle size.

Average length of diagonal lines (L_{mean}) is shown in Figure 13a for PFs and AE signals. As shown in this figure, L_{mean} increases with increasing the average size of particles used in the bed for both PFs and AE signals. It was mentioned previously that determinism indicates percentage of similar states within a system, while L_{mean} can be interpreted as the average time that system visit similar states and named prediction time. Figure 13a illustrates that in the presence of larger particles, fluidized bed views the same states for longer times. As indicated before, bubbles become bigger when larger particles are used in the bed. In contrast, more bubbles are formed when the fluidized bed is filled with fine particles. Appearance of small bubbles causes high-frequency but low energy pressure waves, while large bubbles predominantly generate low-frequency pressure waves with higher energy. In the bed of larger particles, the average lifetime of bubbles is longer than bed of fine particles. In other words, eruption, coalescence and splitting phenomena would be happened faster for small bubbles.

Thus, the contribution of bubble passage phenomenon in the PFs generated by larger bubbles would intensify which results in increasing the mean time that fluidized bed visits the same state (here the same state is bubble passage). In the dynamical point of view, the bubble passage behavior is more predictable than bubble eruption, coalescence and splitting, therefore the PFs generated by larger bubbles can be predicted for a longer time.

The same trend can be observed for L_{mean} of AE signals, which is being due to increase of contribution of particles motion in the bubble phase when larger particles are used in the bed. This figure also demonstrates that L_{mean} of PFs is greater than that of AE signals which indicates that the prediction time of PFs is longer due to the fact that PFs mainly reflect phenomena in the bed which can be predicted for a longer time. He et al.[50] indicated that most energy of AE signals comes mainly from micro-scale structures (interaction among single particles and fluid) and is over 95% of the total energy of the signal. On the other hand, Zhao and Yang[49] concluded that most of the energy of pressure signals is mainly originated from meso-scale structures (clusters and bubbles) and is over 90% of the total energy. Since hydrodynamic behavior of bubbles and clusters is more predictable than single particles, the mean time that PFs can be predicted is longer than that for AE signals. In other words, motion of bubbles is more predictable than motion of particles.

Figure 13b reveals that the trapping time has an increasing trend for both PFs and AE signals as the particle sizes increases. Since trapping time indicates the mean time that the system remain in a certain state, it can be concluded that in a fluidized bed of larger particles, the bed repeats its dynamical behavior for a longer time than for smaller particles. As indicated before, PFs in a bubbling fluidized bed predominantly reflect hydrodynamic characteristics, such as bubble passage and eruption. The average lifetime of larger bubbles is longer in the bed of larger

particles (lager bubble generates lower frequency waves). This means that the characteristics reflected in PFs would be repeated (or trapped in a certain state) for a longer time in the bed of larger particles. In other words, the dynamic state of the bed would be trapped in the time of bubble generation up to bubble eruption or coalescence and this time is longer for larger bubbles. As discussed before, interconnection space (stagnant zones) between two circulation zones increases when the size of particles is increased. Moreover, the size of cloud of recirculation gas surrounding the bubble increases with increasing size of bed particles.[53] Thus, the number of particles carried out in the wake of larger bubbles would increase. Also, Hoffmann et al.[54] concluded that the total volumetric flow rate of material in and out of the bubble wake is proportional to the size of the wake/bulk interface, which means that more particles would be taken up in the wake of larger bubbles. Therefore, the amount of particles circulating in the emulsion phase and their number of collisions decrease in the bed of larger particles. This leads to increase in the AE trapping times, because in the presence of less number of circulating particles, the collisions would happen after a longer time.

Also, it can be seen in Figure 13b that the trapping time for PFs is greater than that for the AE signals. This is due to the fact that AE of a gas-solid fluidized bed mainly arise from particle-particle and particle-wall collisions and reflects the interactions among particles. In contrast, PFs are mainly generated by movement of bubbles. Interactions among bubbles (macro structure) take a longer time than collisions of particles (micro structure) which means that PF are repeated after a longer time than AE signals.

Comparison with conventional non-linear analysis method

Various methods have been proposed in literature for detection of particle size changes in fluidized beds. Among these methods, comparison of attractors based on the S-statistic method[7] provides a proper accuracy and acceptability. Therefore, to test the method proposed in this work, its results were compared with those of the S-statistic. The S-statistic is based on a statistical test proposed by Diks et al.[55] that compares two attractors by evaluating the dimensionless squared distance S between the two attractors. The S-value is calculated from:[7]

$$S = \frac{\hat{Q}}{\sqrt{V_C(\hat{Q})}} \tag{10}$$

where $\hat{Q}$ is the unbiased estimator of the squared distance between two delay vector distributions in the state space and $V_C(\hat{Q})$ is the variance of $\hat{Q}$. When comparing two signals obtained from the same hydrodynamic conditions, the S-statistic method can show this similarity of attractors with an S-value close to zero. On the other hand, when comparing two signals measured at different operating conditions, an S-value greater than 3 indicates, with more 95% confidence, that there exist two different attractors in this case.[7] Performance of the S-statistic method depends on appropriate selection of four input parameters: embedding dimension (m), bandwidth (d), segment length (l_s) and time window (T_w). Here, time window is the time span described by one delay vector. Attractor reconstruction in this method is the same as discussed in the RP reconstruction section, except that it moves with step size m through the time series instead of with step size one; this makes the total calculation procedure a factor m^2 times faster.[7] These parameters were optimized according to the procedure described by van Ommen et al.[7] and the optimum values used in this work for both PFs and AE signals are given in Table 3.

The S-value as a function of average particle size, calculated for PFs and AE signals, at various superficial gas velocities are shown in Figure 14. It can be seen in this figure that the S-

value is less than 3 in the bed of 5% sand type II in sand type I which indicates that the S-statistic method is not able to detect 10 μm changes in the particle size. This value for AE signals crosses the threshold value of $S = 3$ for 22 μm changes in average particle size (change from 368 to 390 μm) while for PFs this value is less than 3. The S-values are greater than 3 for both PFs and AE signals at average particle size change from 368 to 402 μm. This trend shows that the S-statistic can detect large changes in average particle size (higher than 22 μm) at lower superficial gas velocities. On the other hand, the RQA shows good sensitivity to smaller changes in the particle size (10 μm) at high superficial gas velocities. While the sensitivity of both PFs and AE signals based on the S-statistic to particle size changes is reduced at higher gas velocities, the sensitivity of the RQA method to changes in the average particle size remained constant.

The main advantage of the RP method to the S-statistic method is that parameters of RP method can be set easier. As mentioned before, calculations in the RP method needs only the radius threshold whereas in the calculation of S-statistic three input parameters should be set (embedding dimension, bandwidth and segment length). The radius threshold can be selected easily in the RP method while embedding dimension, band width and segment length in the S-statistic method are difficult to calculate and need to be optimized. Thus, it can be concluded that input parameter setting in the RP method is faster and simpler than in the S-statistic method. Values of input parameters and comparison of the both methods are summarized in Table 4. This table clearly shows that calculation in the RP method is numerically simpler than in the S-statistic method. Moreover, the S-statistic method is based on comparison of a reference time series with the one measured during the operation (evaluation time series). Proper selection of the reference time series is a critical step in this method and it should adequately reflect the required or optimum state of the bed hydrodynamics.[7] In contrast, the RQA method is based on

auto-comparison of measured signal and this feature eliminates the need for reference time series, which shows the ease of use of this method when compared to the S-statistic. In addition, the minimum number of data points needed in the S-statistic method (65,535 for PFs and 2,157,745 for AE) is much more than those needed in the RP method (3000 for PFs and 5000 for AE). The smaller number of data points for calculations of the RP method, results in shorter calculation time. The smaller number of data points also eliminates the problem associated with long-term data sampling. As pointed out before, despite the smaller number of data points, the RP method shows higher sensitivity to small changes in particle size, especially at high superficial gas velocities.

Conclusions

This study represents the application of recurrence plot (RP) and recurrence quantification analysis (RQA) for detecting small changes in particle size of fluidized beds. Pressure fluctuations (PFs) and acoustic emissions (AE) of fluidized beds were considered as time series. RP structures and RQA parameters were investigated at various gas velocities and particle sizes. The main findings of the present study can be summarized as follows:

- Structures in RP of PFs and AE signals can be classified into two groups: local white areas (LWA) and local bold areas (LBA). Variations of their patterns can be recognized visually for AE-RPs when particle size changes, while these variations cannot be distinguished graphically for RPs of PFs. Moreover, variations in the size of LWAs and LBAs against particle size at higher gas velocities are more drastic for AE signals.
- RQA parameters were investigated in order to quantify the small-scale structures in RPs. It was found that recurrence rate (for both PFs and acoustic signals) decrease with

increasing the average particle size. This behavior confirms the graphical variations of RP structures for AE signals at different particles sizes. Also, this trend implies that although the variations of LWA and LBA in PFs-RP structures are not easily visible; the RQA parameters of PFs vary with particle size changes.

- In the bubbling regime of fluidization, the contribution of macro structures increases when larger particles added to the bed. This trend was confirmed by the RQA method. DET, LAM, L_{mean} and TT increase when mean diameter of particles increases. Sensitivity of these parameters to small changes in particle size illustrates the applicability of the RQA method to particle size monitoring in different fluidized bed processes, such as coating, granulation, drying and gasification.
- Based on thorough investigation of RP structures and RQA parameters of both PFs and AE signals measured in gas-solid fluidized bed, it was shown that AE measurement technique could be a reliable method for detecting the particle-related changes in gas-solid fluidized bed, such as detection of particle size changes. In contrast, the PFs mainly reflect the dynamics of gas phase.
- Based on RQA parameters of PFs and AE signals, it was concluded that PFs are more predictable and simpler than AE signals. This means that dynamics of bubble and gas phase is more predictable and simpler than particle motion in gas-solid fluidized bed.
- While both RP and S-statistic methods are selectively sensitive to changes in the mean particle size, the sensitivity of RP method is more than S-statistic method.

Notation

DET = determinism

$D_{i,j}$ = elements of distance matrix

d = band width

d_p = average particle diameter

l = diagonal line parameter

l_s = segment length

L = epoch length

L/D = height to bed ratio of fluidized bed

L_{mean} = average diagonal line length

LAM = laminarity

m = embedding dimension

N = number of data points

N_l = number of diagonal lines

$P(l)$ = number of diagonal lines of length l

$P(v)$ = number of vertical lines of length ν

$R_{i,j}$ = recurrence plot matrix

RR = recurrence rate

T_w = time window

TT = trapping time

U = superficial gas velocity

U_{mf} = minimum fluidization velocity

U_c = turbulent fluidization velocity

$\overrightarrow{x_i}$ = *i*-th point of state space trajectory

Greek letters

Θ = Heaviside function

ε = radius threshold

υ = vertical line parameter

τ = time delay vector

Literature Cited

1. Kunii D, Levenspiel O. *Fluidization engineering*. (2nd edition). Butterworth-Heinemann serieis in chemical engineering, Elsevier; 1991.
2. Cai P, Jin Y, Yu ZQ, Wang ZW. Mechanism of flow regime transition from bubbling to turbulent fluidization. *AlChE J.* 1990;36(6):955-956.
3. Fan L, Ho TC, Hiraoka S, Walawender W. Pressure fluctuations in a fluidized bed. *AlChE J.* 1981;27(3):388-396.
4. Dehkordi AM, Savari C, Ghasemi M. Steam reforming of methane in a tapered membrane–assisted fluidized–bed reactor: modeling and simulation. *Int J Hydrogen Energy*. 2011;36(1):490-504.
5. Van der Schaaf J, Van Ommen J, Takens F, Schouten J, van den Bleek C. Similarity between chaos analysis and frequency analysis of pressure fluctuations in fluidized beds. *Chem Eng Sci.* 2004;59(8):1829-1840.
6. Zhou Y, Ren C, Wang J, Yang Y. Characterization on hydrodynamic behavior in liquid-containing gas-solid fluidized bed reactor. *AIChE J.* 2013;59(4):1056-1065.
7. van Ommen JR, Coppens MO, van den Bleek CM, Schouten JC. Early warning of agglomeration in fluidized beds by attractor comparison. *AIChE J*. 2000;46(11):2183-2197.
8. Schouten JC, van den Bleek CM. Monitoring the quality of fluidization using the short-term predictability of pressure fluctuations. *AIChE J.* 1998;44(1):48.
9. Hemati M, Cherif R, Saleh K, Pont V. Fluidized bed coating and granulation: influence of process-related variables and physicochemical properties on the growth kinetics. *Powder Technol.* 2003;130(1):18-34.

10. Saleh K, Steinmetz D, Hemati M. Experimental study and modeling of fluidized bed coating and agglomeration. *Powder Technol.* 2003;130(1):116-123.

11. Dernedde M, Peglow M, Tsotsas E. A novel, structure-tracking monte carlo algorithm for spray fluidized bed agglomeration. *AIChE J.* 2012;58(10):3016-3029.

12. Abbasi M, Sotudeh-Gharebagh R, Mostoufi N, Zarghami R, Mahjoob M. Nonintrusive characterization of fluidized bed hydrodynamics using vibration signature analysis. *AIChE J.* 2010;56(3):597-603.

13. Abbasi M, Sotudeh-Gharebagh R, Mostoufi N, Mahjoob M. Non-intrusive monitoring of bubbles in a gas–solid fluidized bed using vibration signature analysis. *Powder Technol.* 2009;196(3):278-285.

14. Zarghami R, Mostoufi N, Sotudeh-Gharebagh R. Nonlinear characterization of pressure fluctuations in fluidized beds. *Ind Eng Chem Res.* 2008;47(23):9497-9507.

15. Song J, Fan L, Yutani N. Fault detection of the fluidized bed distributor by pressure fluctuation signal. *Chem Eng Commun.* 1984;25(1-6):105-116.

16. Bartels M, Lin W, Nijenhuis J, Kapteijn F, van Ommen JR. Agglomeration in fluidized beds at high temperatures: Mechanisms, detection and prevention. *Prog Energy Combust Sci.* 2008;34(5):633-666.

17. Chong Y-O, O'Dea D, White ET, Lee PL, Leung LS. Control of the quality of fluidization in a tall bed using the variance of pressure fluctuations. *Powder Technol.* 1987;53(3):237-246.

18. Azizpour H, Sotudeh-Gharebagh R, Zarghami R, Abbasi M, Mostoufi N, Mahjoob M. Characterization of gas–solid fluidized bed hydrodynamics by vibration signature analysis. *Int J Multiphase Flow.* 2011;37(7):788-793.

19. Briens L, Daniher D, Tallevi A. Monitoring high-shear granulation using sound and vibration measurements. *Int J Pharm.* 2007;331(1):54-60.

20. Briongos JV, Aragón JM, Palancar MC. Fluidised bed dynamics diagnosis from measurements of low-frequency out-bed passive acoustic emissions. *Powder Technol.* 2006;162(2):145-156.

21. Hansuld EM, Briens L, McCann JA, Sayani A. Audible acoustics in high-shear wet granulation: Application of frequency filtering. *Int J Pharm.* 2009;378(1):37-44.

22. Gamble JF, Dennis AB, Tobyn M. Monitoring and end-point prediction of a small scale wet granulation process using acoustic emission. *Pharm Dev Technol.* 2009;14(3):299-304.

23. Tsujimoto H, Yokoyama T, Huang C, Sekiguchi I. Monitoring particle fluidization in a fluidized bed granulator with an acoustic emission sensor. *Powder Technol.* 2000;113(1):88-96.

24. Salehi-Nik N, Sotudeh-Gharebagh R, Mostoufi N, Zarghami R, Mahjoob M. Determination of hydrodynamic behavior of gas–solid fluidized beds using statistical analysis of acoustic emissions. *Int J Multiphase Flow.* 2009;35(11):1011-1016.

25. Van der Schaaf J, Schouten J, Johnsson F, Van den Bleek C. Non-intrusive determination of bubble and slug length scales in fluidized beds by decomposition of the power spectral density of pressure time series. *Int J Multiphase Flow.* 2002;28(5):865-880.

26. Trnka O, Veselý V, Hartman M, Beran Z. Identification of the state of a fluidized bed by pressure fluctuations. *AIChE J.* 2000;46(3):509-514.

27. Chaplin G, Pugsley T, Winters C. Application of chaos analysis to pressure fluctuation data from a fluidized bed dryer containing pharmaceutical granule. *Powder Technol.* 2004;142(2):110-120.

28. Eckmann J-P, Kamphorst SO, Ruelle D. Recurrence plots of dynamical systems. *Europhys Lett.* 1987;4(9):973-977.

29. Babaei B, Zarghami R, Sedighikamal H, Sotudeh-Gharebagh R, Mostoufi N. Investigating the hydrodynamics of gas–solid bubbling fluidization using recurrence plot. *Adv Powder Technol.* 2012;23(3):380-386.

30. Tahmasebpour M, Zarghami R, Sotudeh-Gharebagh R, Mostoufi N. Characterization of various structures in gas-solid fluidized beds by recurrence quantification analysis. *Particuology.* 2013;11(6):647-656.

31. Tahmasebpoor M, Zarghami R, Sotudeh-Gharebagh R, Mostoufi N. Characterization of fluidized beds hydrodynamics by recurrence quantification analysis and wavelet transform. *Int J Multiphase Flow.* 2015;69:31-41.

32. Babaei B, Zarghami R, Sotudeh-Gharebagh R. Monitoring of fluidized beds hydrodynamics using recurrence quantification analysis. *AIChE J.* 2013;59(2):399-406.

33. Johnsson F, Zijerveld R, Schouten J, Van den Bleek C, Leckner B. Characterization of fluidization regimes by time-series analysis of pressure fluctuations. *Int J Multiphase Flow.* 2000;26(4):663-715.

34. Vander Stappen MLM. *Chaotic hydrodynamics of fluidized beds*: TU Delft, Delft University of Technology; 1996.

35. March T, Chapman S, Dendy R. Recurrence plot statistics and the effect of embedding. *Physica D.* 2005;200(1):171-184.

36. Amigó JM, Szczepański J, Wajnryb E, Sanchez-Vives MV. Estimating the entropy rate of spike trains via Lempel-Ziv complexity. *Neural Comput.* 2004;16(4):717-736.

37. Marwan N, Romano MC, Thiel M, Kurths J. Recurrence plots for the analysis of complex systems. *Phys. Rep.* 2007;438(5):237-329.

38. Takens F. *Detecting strange attractors in turbulence*: Springer; 1981.

39. Marwan N, Wessel N, Meyerfeldt U, Schirdewan A, Kurths J. Recurrence-plot-based measures of complexity and their application to heart-rate-variability data. *Phys. Rev. E.* 2002;66(2):026702.

40. Webber CL, Zbilut JP. Dynamical assessment of physiological systems and states using recurrence plot strategies. *Eur. J. Appl. Physiol. European.* 1994;76(2):965-973.

41. Webber Jr CL, Zbilut JP. Recurrence quantification analysis of nonlinear dynamical systems. In: Riley MA, Van Orden GC (Eds.). *Tutorials in contemporary nonlinear methods for the behavioral sciences.* 2005:26-94. Available at: http://www.nsf.gov/sbe/bcs/pac/nmbs/nmbs.jsp

42. Gandhi A, Joshi J, Kulkarni A, Jayaraman V, Kulkarni B. SVR-based prediction of point gas hold-up for bubble column reactor through recurrence quantification analysis of LDA time-series. *Int J Multiphase Flow.* 2008;34(12):1099-1107.

43. Tahmasebpour M, Zarghami R, Sotudeh-Gharebagh R, Mostoufi N. Study of transition velocity from fluidization by recurrence plots analysis on pressure fluctuations. *Can J Chem Eng*. 2013;91(2):368-375.

44. Sedighikamal H, Zarghami R. Dynamic characterization of bubbling fluidization through recurrence rate analysis of pressure fluctuations. *Particuology*. 2013;11(3):282-287.

45. Iwanski JS, Bradley E. Recurrence plots of experimental data: To embed or not to embed? *Chaos*. 1998;8(4):861-871.

46. Thiel M, Romano M, Read P, Kurths J. Estimation of dynamical invariants without embedding by recurrence plots. *Chaos.* 2004;14(2):234-243.

47. Fraser AM, Swinney HL. Independent coordinates for strange attractors from mutual information. *Phys Rev A.* 1986;33(2):1134.

48. Babaei B, Zarghami R, Sedighikamal H, Sotudeh-Gharebagh R, Mostoufi N. Selection of minimal length of line in recurrence quantification analysis. *Physica A.* 2014;395:112-120.

49.Zhao GB, Yang YR. Multiscale resolution of fluidized-bed pressure fluctuations. *AIChE J.* 2003;49(4):869-882.

50. He YJ, Wang JD, Cao YJ, Yang YR. Resolution of structure characteristics of AE signals in multiphase flow system-from data to information. *AIChE J.* 2009;55(10):2563-2577.

51. Constantinides A, Mostoufi N. *Numerical Methods for Chemical Engineers with MATLAB Applications*. New York: Prentice Hall PTR, 1999.

52. Wang J, Ren C, Yang Y, Hou L. Characterization of particle fluidization pattern in a gas solid fluidized bed based on acoustic emission (AE) measurement. *Ind Eng Chem Res.* 2009;48(18):8508-8514.

53. Harrison D, Leung L. Bubble formation at an orifice in a fluidized bed. 1961.

54. Hoffmann A, Janssen L, Prins J. Particle segregation in fluidised binary mixtures. *Chem Eng Sci.* 1993;48(9):1583-1592.

55. Diks C, Van Zwet W, Takens F, DeGoede J. Detecting differences between delay vector distributions. *Phys. Rev. E.* 1996;53(3):2169.

Table 1. Optimal input parameters in the RQA

Input parameter	PF	AE
Epoch length (L)	7.5 s (3000 points)	114 ms (5000 points)
Embedding dimension (m)	1	1
Time delay (τ)	1	1
Radius threshold (ε)	0.05	0.05
Minimal length of diagonal line (l_{min})	2	2
Minimal length of diagonal line (υ_{min})	2	2

Table 2. Minumum fluidization veloicity and gas velocity at onset of turbulent regime for particle mixtures used in the experiments[1]

	U_{mf} (m/s)	U_c (m/s)
100% sand type I (d_p=368 μm)	0.10	0.80
5 % sand type I + 95% sand type II (d_p=378 μm)	0.11	0.83
10 % sand type I + 90% sand type II (d_p=390 μm)	0.12	0.86
15 % sand type I + 85% sand type II (d_p=402 μm)	0.14	0.90

Table 3. Optimal input parameters in the S-statistic method

Signals	Embedding dimension (m)	Band width (d)	Segment length (l_s)	Time window (T_w)
PF	20	0.5	5 s	50 ms
AE	18	0.7	6 s	0.41 ms

Table 4. Comparison of RP and S-statistic methods

	S-Statistic method	RP method
Parameter settings	Three input parameters: embedding dimension (time window), band width, segment length	Only one input parameter: radius threshold
Embedding dimension	20 for PF and 18 for AE	No embedding
Length of the signal	Minimum 65,535 for PF and 2,200,000 for AE	3000 for PF and 5000 for AE
Complexity of the calculations	More complex	Simpler
Sensitivity to particle size changes	PFs can detect 34 μm change in average particle size AE can detect 22 μm change in average particle size	Both PFs and AE can detect 10 μm change in average particle size

Figure Captions

Figure 1. Recurrence plot reconstruction.

Figure 2. Evolution of recurrence rate and determinism versus the number of data points at U= 0.2 m/s, m=1, τ=1, ε=0.05, (a) and (b) for PFs, (c) and (d) for AE.

Figure 3. Recurrence plots of PFs of fluidized bed at U=0.2 m/s, τ=1, ε=0. 5 (a) m=1, (b) m=2, (c) m=4 and (d) m=10.

Figure 4. Recurrence plots of AE signals of fluidized bed at U=0.2 m/s, τ=1, ε=1 (a) m=1, (b) m=2, (c) m=4 and (d) m=10.

Figure 5. Determinism and laminarity of PFs and AE signals versus average particle size at U=0.2 m/s, τ=1 and different embedding dimension.

Figure 6. Full logarithmic plot of recurrence rate and determinism versus radius threshold at U=0.2 m/s, τ=1, m=1.

Figure 7. Recurrence plots of PFs of fluidized bed at superficial gas velocity of 0.2 m/s for (a) sand type I, (b) 95% sand type I + 5% sand type II, (c) 90% sand type I + 10% sand type II and (d) 90% sand type I + 15% sand type II, (m=1, τ=1, ε=0. 5).

Figure 8. Recurrence plots of AE signals of fluidized bed at superficial gas velocity of 0.2 m/s for (a) sand type I, (b) 95% sand type I + 5% sand type II, (c) 90% sand type I + 10% sand type II and (d) 90% sand type I + 15% sand type II, (m=1, τ=1, ε=1).

Figure 9. Recurrence plots of PFs of fluidized bed at superficial gas velocity of 0.6 m/s for (a) sand type I, (b) 95% sand type I + 5% sand type II, (c) 90% sand type I + 10% sand type II and (d) 90% sand type I + 15% sand type II, (m=1, τ=1, ε=0.5).

Figure 10. Recurrence plots of AE signals of fluidized bed at superficial gas velocity of 0.6 m/s for (a) sand type I, (b) 95% sand type I + 5% sand type II, (c) 90% sand type I + 10% sand type II and (d) 90% sand type I + 15% sand type II, (m=1, τ=1, ε=1).

Figure 11. Recurrence rate versus average particle size for PFs and AE signal at m=1, τ=1, ε=0.05.

Figure 12. Determinism and laminarity versus average particle size for PFs and AE signal at m=1, τ=1, ε=0.05.

Figure 13. Average length of diagonal lines and trapping time versus average particle size for PFs and AE signal at m=1, τ=1, ε=0.05.

Figure 14. S-value versus average particle size for PFs and AE signal.

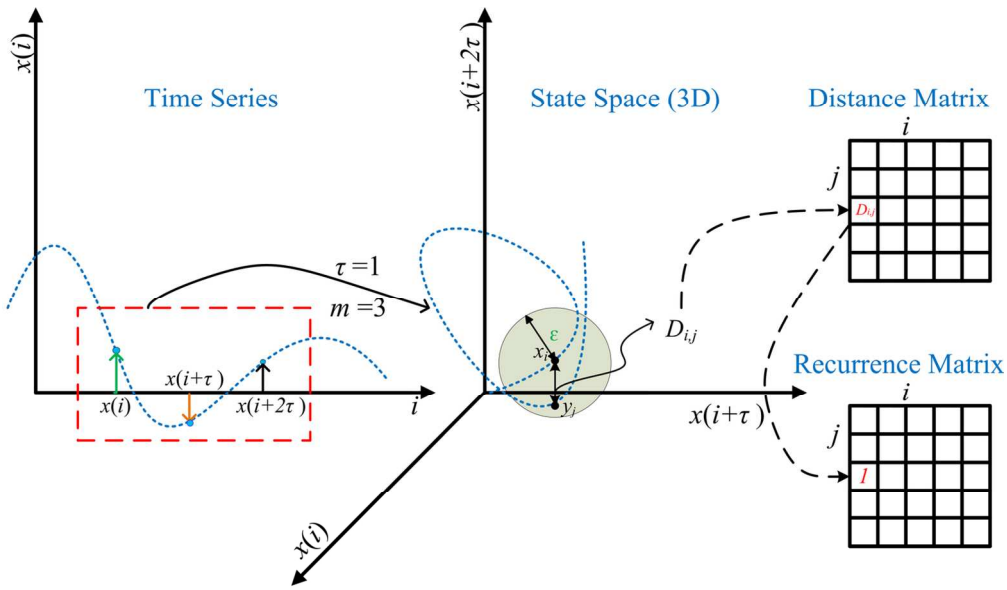

Figure 1. Recurrence plot reconstruction.
131x76mm (300 x 300 DPI)

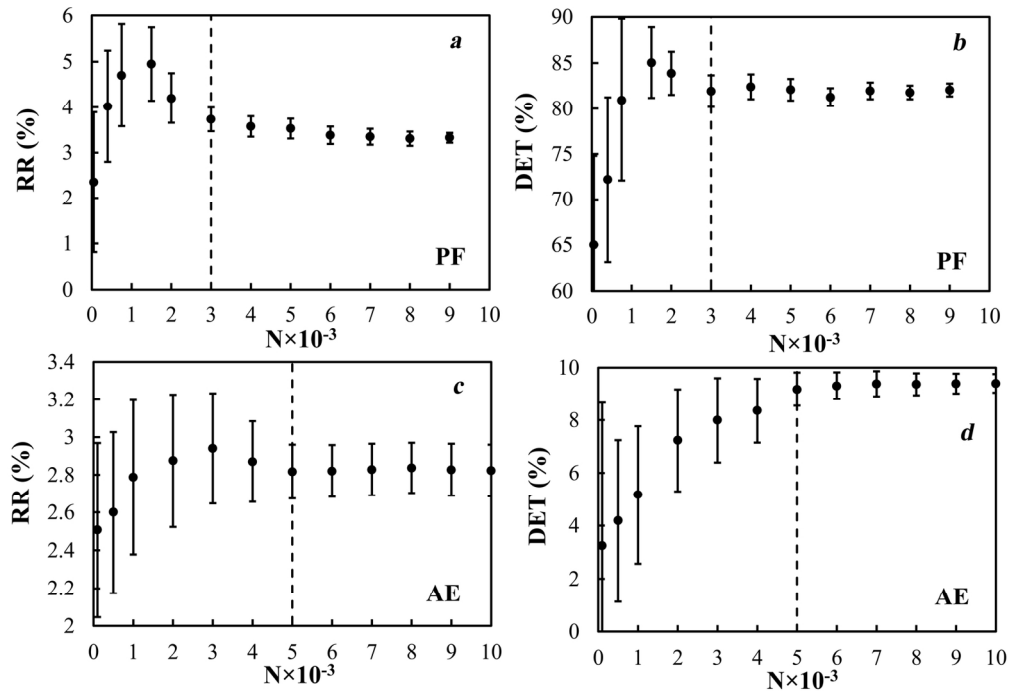

Figure 2. Evolution of recurrence rate and determinism versus the number of data points at U= 0.2 m/s, m=1, τ=1, ε=0.05, (a) and (b) for PFs, (c) and (d) for AE.
153x104mm (300 x 300 DPI)

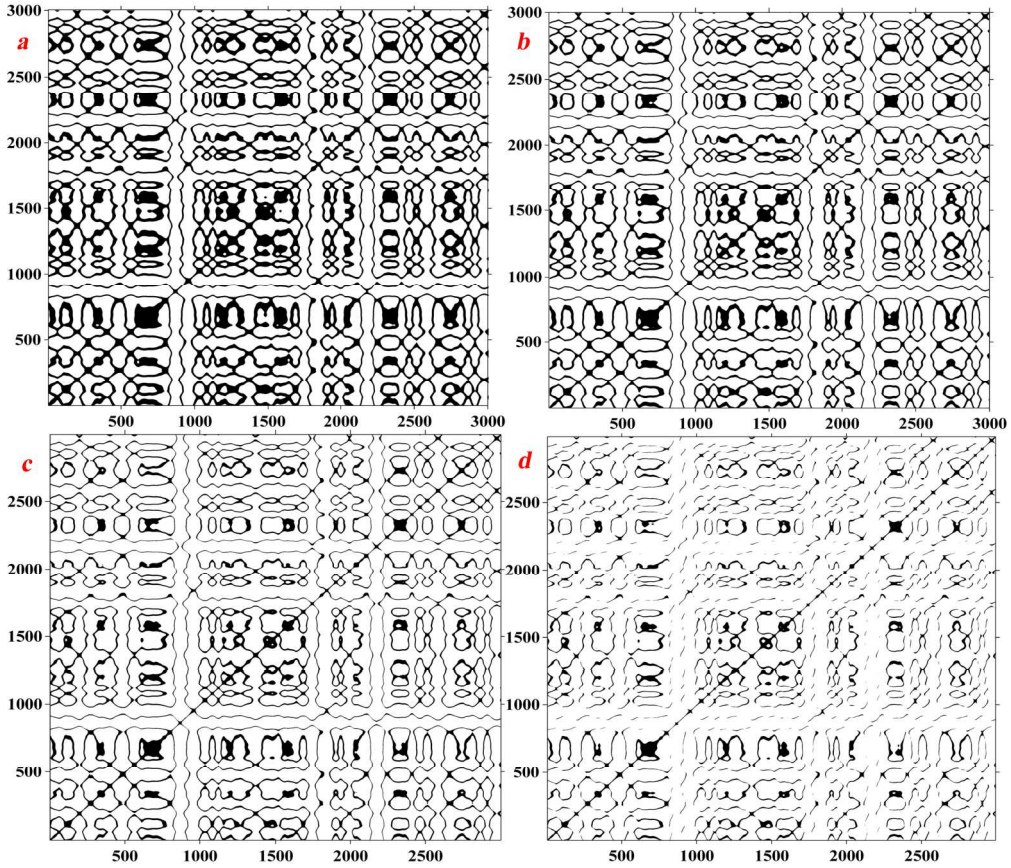

Figure 3. Recurrence plots of PFs of fluidized bed at U=0.2 m/s, τ=1, ε=0. 5 (a) m=1, (b) m=2, (c) m=4 and (d) m=10.
222x192mm (300 x 300 DPI)

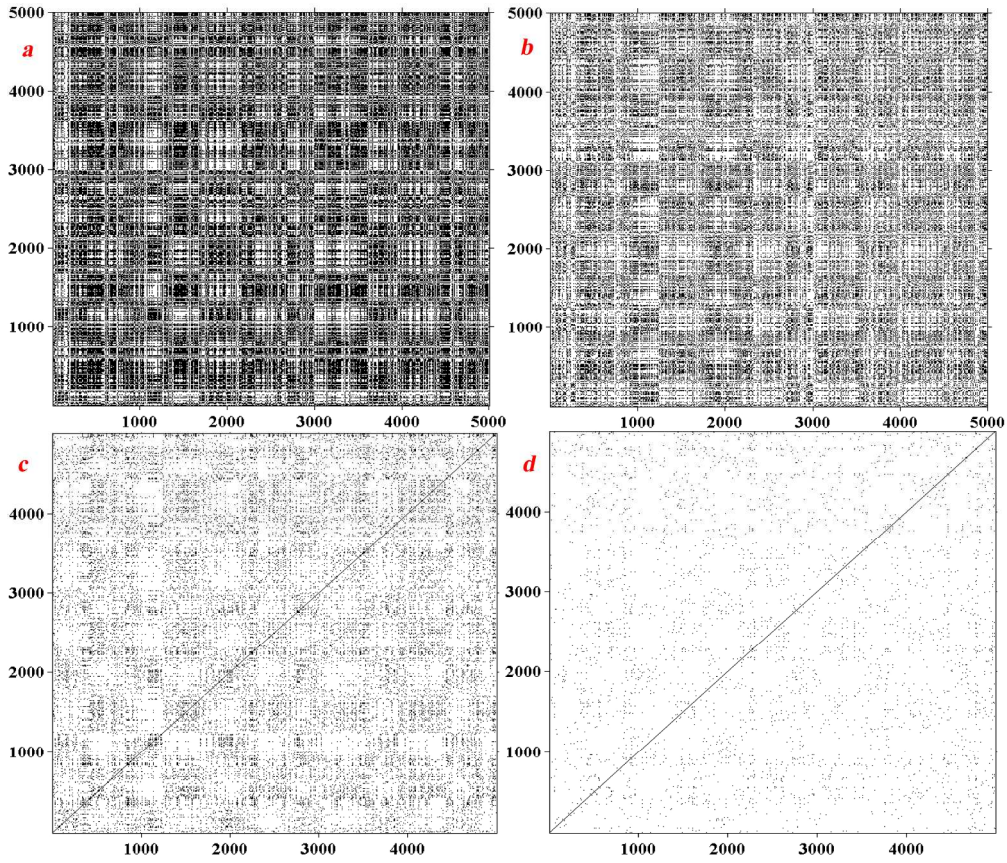

Figure 4. Recurrence plots of AE signals of fluidized bed at U=0.2 m/s, τ=1, ε=1 (a) m=1, (b) m=2, (c) m=4 and (d) m=10.
228x194mm (300 x 300 DPI)

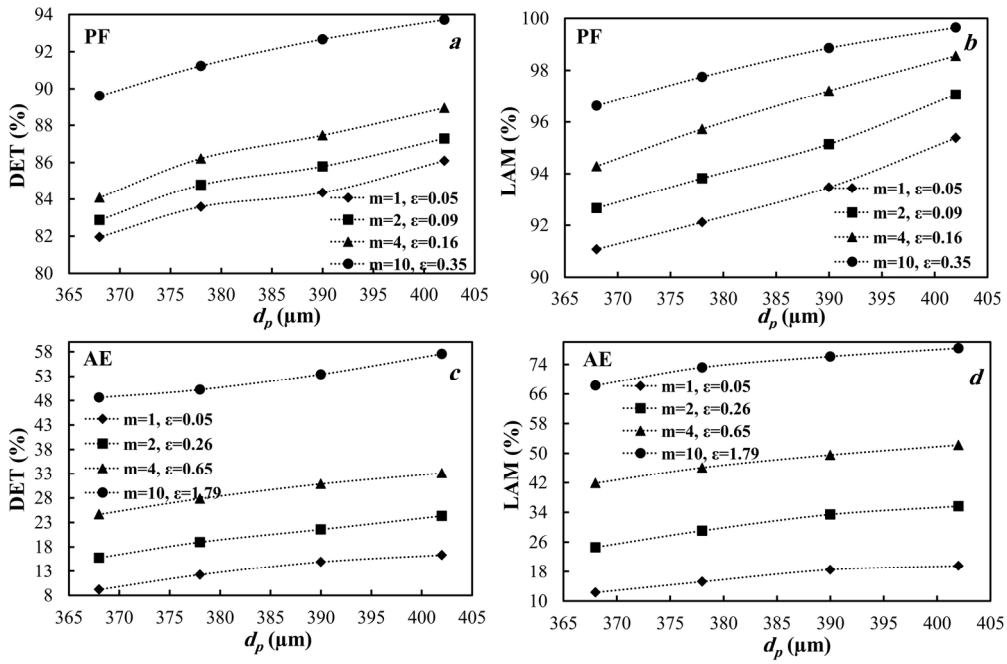

Figure 5. Determinism and laminarity of PFs and AE signals versus average particle size at U=0.2 m/s, τ=1 and different embedding dimension.
173x114mm (300 x 300 DPI)

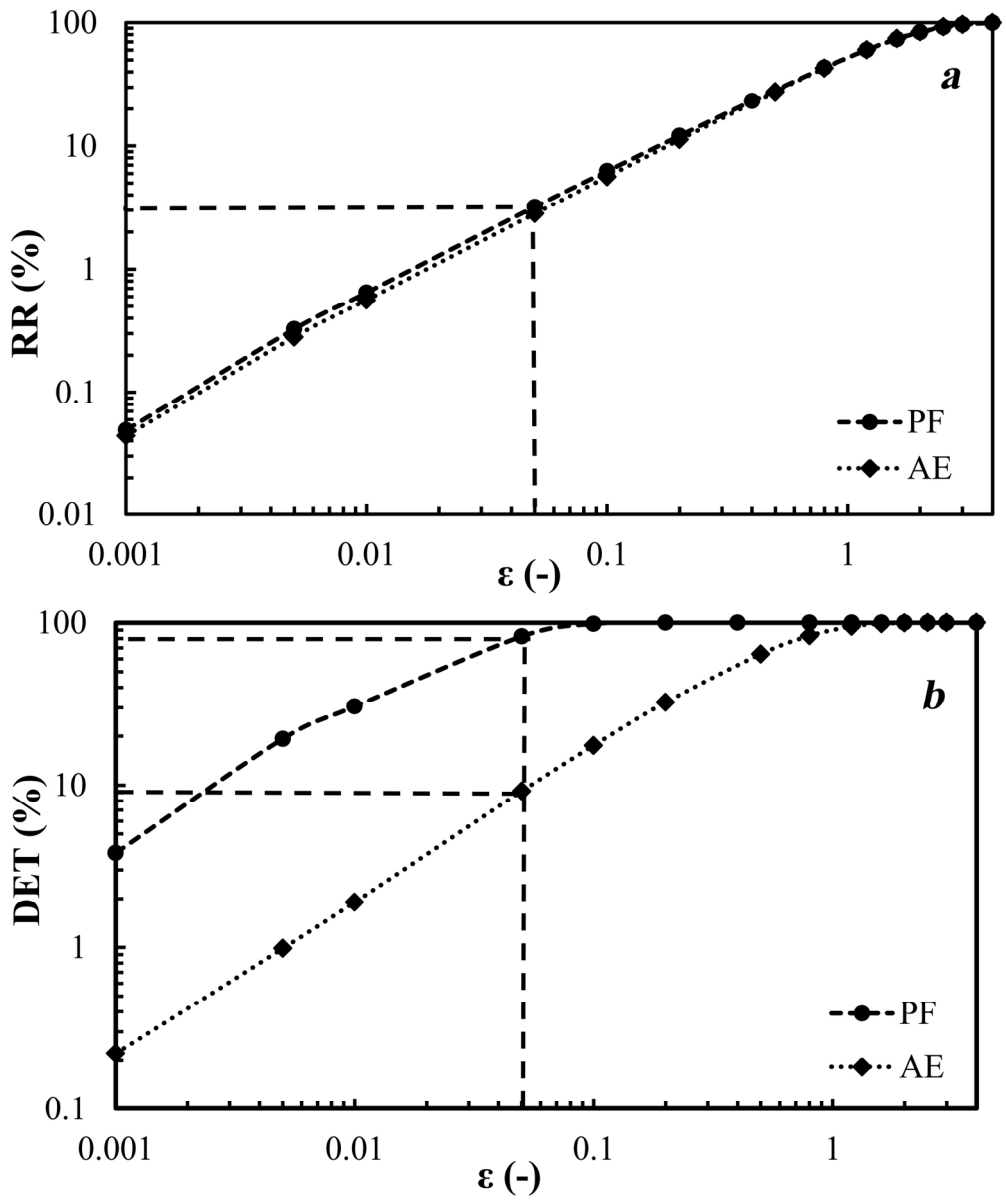

Figure 6. Full logarithmic plot of recurrence rate and determinism versus radius threshold at U=0.2 m/s, τ=1, m=1.
174x209mm (300 x 300 DPI)

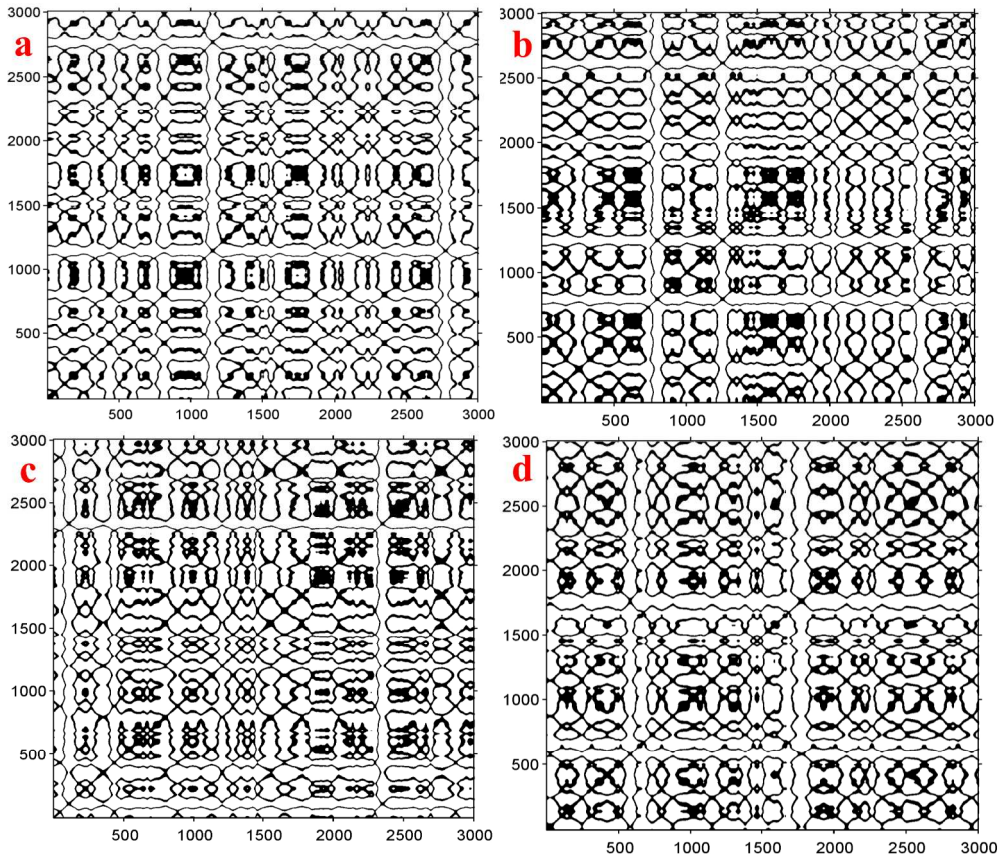

Figure 7. Recurrence plots of PFs of fluidized bed at superficial gas velocity of 0.2 m/s for (a) sand type I, (b) 95% sand type I + 5% sand type II, (c) 90% sand type I + 10% sand type II and (d) 90% sand type I + 15% sand type II, (m=1, τ=1, ε=0. 5).
251x215mm (300 x 300 DPI)

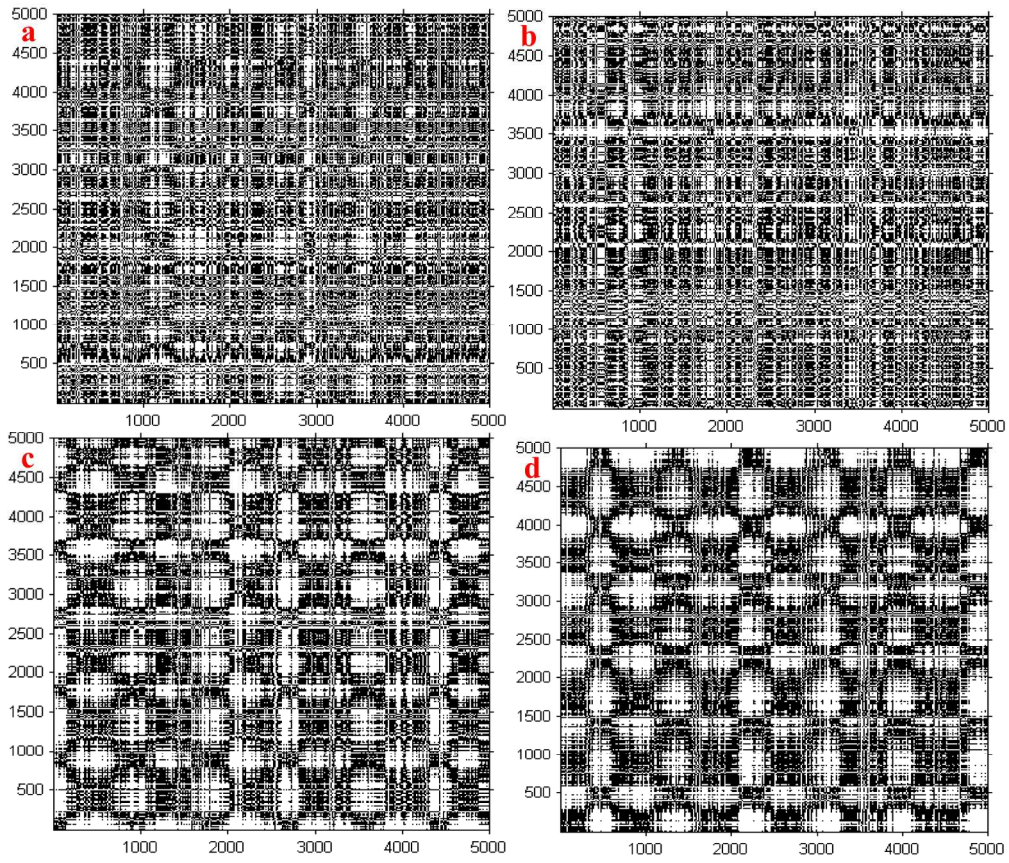

Figure 8. Recurrence plots of AE signals of fluidized bed at superficial gas velocity of 0.2 m/s for (a) sand type I, (b) 95% sand type I + 5% sand type II, (c) 90% sand type I + 10% sand type II and (d) 90% sand type I + 15% sand type II, (m=1, τ=1, ε=1).
196x167mm (300 x 300 DPI)

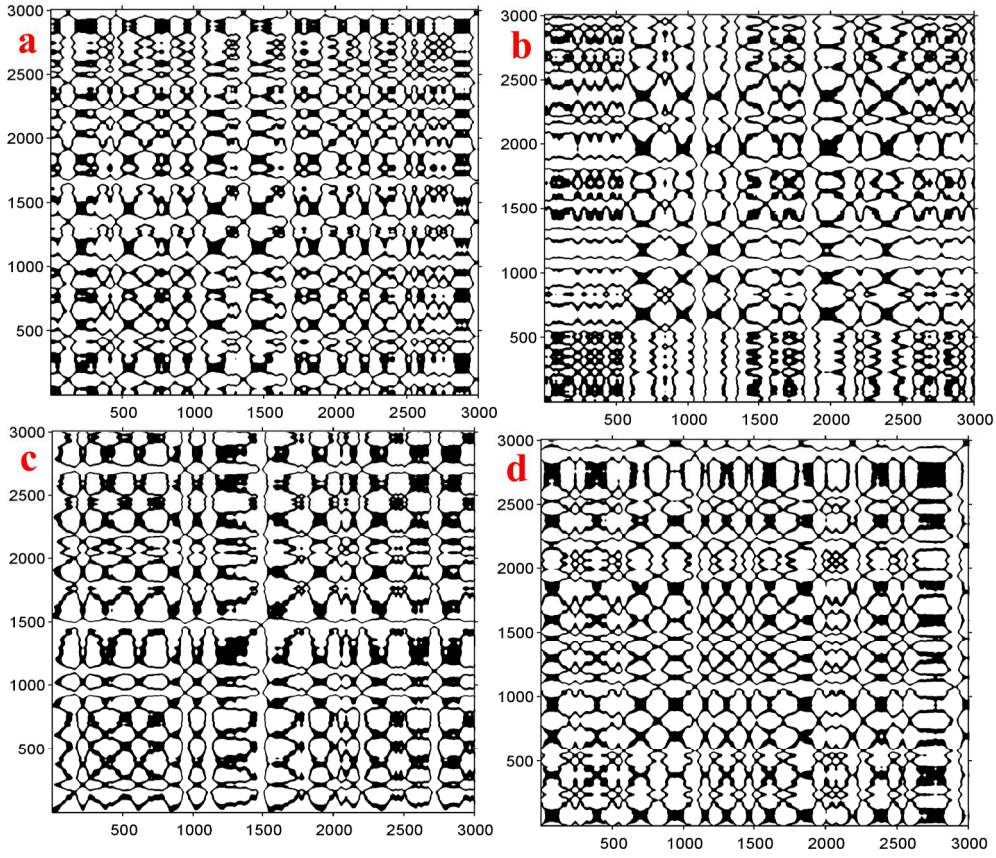

Figure 9. Recurrence plots of PFs of fluidized bed at superficial gas velocity of 0.6 m/s for (a) sand type I, (b) 95% sand type I + 5% sand type II, (c) 90% sand type I + 10% sand type II and (d) 90% sand type I + 15% sand type II, (m=1, τ=1, ε=0.5).
246x211mm (300 x 300 DPI)

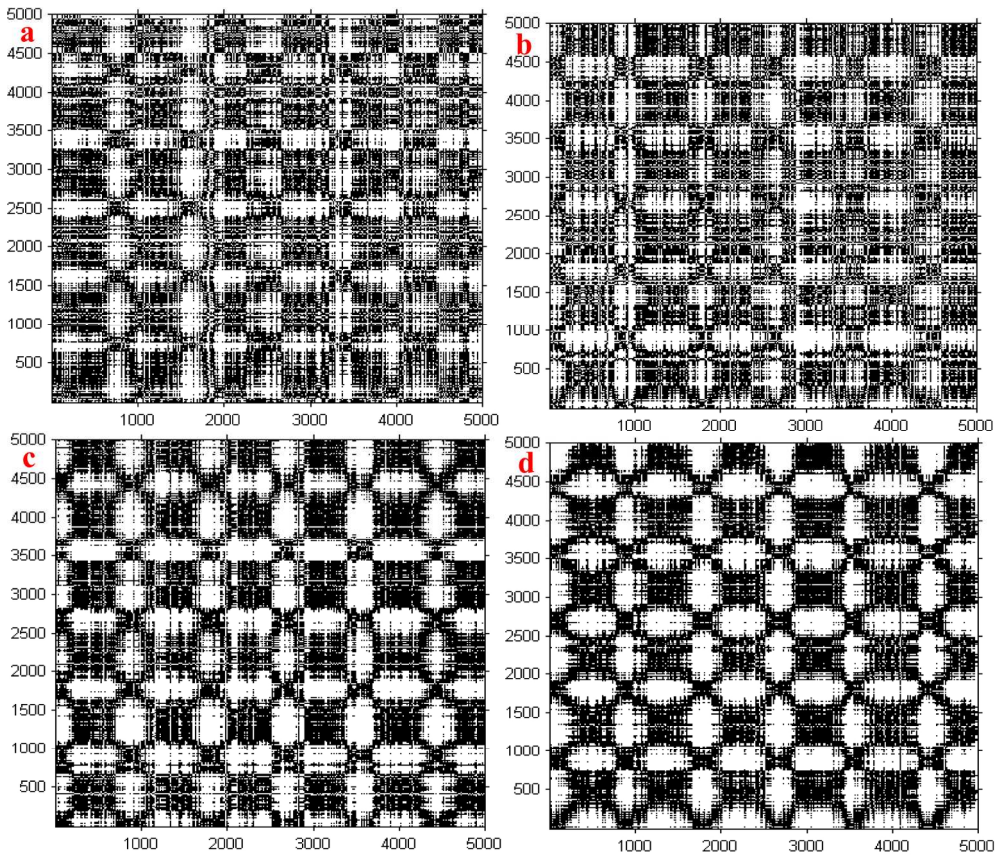

Figure 10. Recurrence plots of AE signals of fluidized bed at superficial gas velocity of 0.6 m/s for (a) sand type I, (b) 95% sand type I + 5% sand type II, (c) 90% sand type I + 10% sand type II and (d) 90% sand type I + 15% sand type II, (m=1, τ=1, ε=1).
193x163mm (300 x 300 DPI)

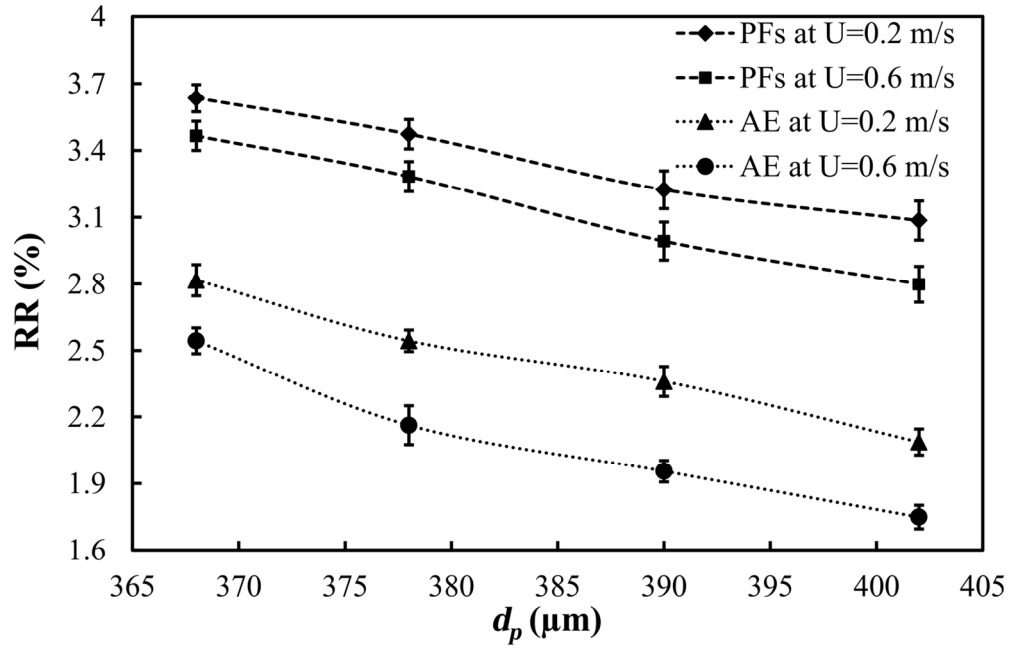

Figure 11. Recurrence rate versus average particle size for PFs and AE signal at m=1, τ=1, ε=0.05.
136x87mm (300 x 300 DPI)

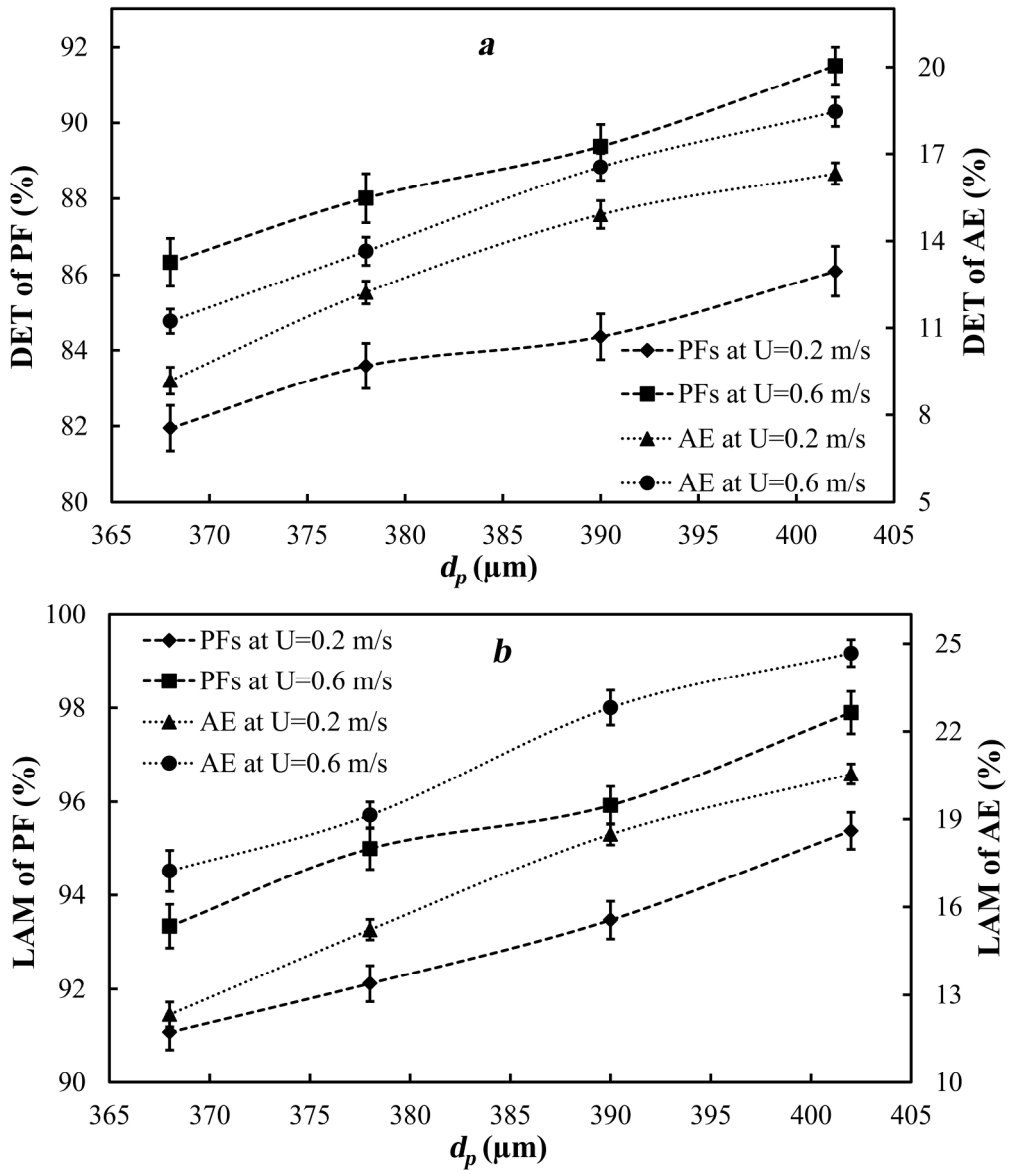

Figure 12. Determinism and laminarity versus average particle size for PFs and AE signal at m=1, τ=1, ε=0.05.
210x249mm (300 x 300 DPI)

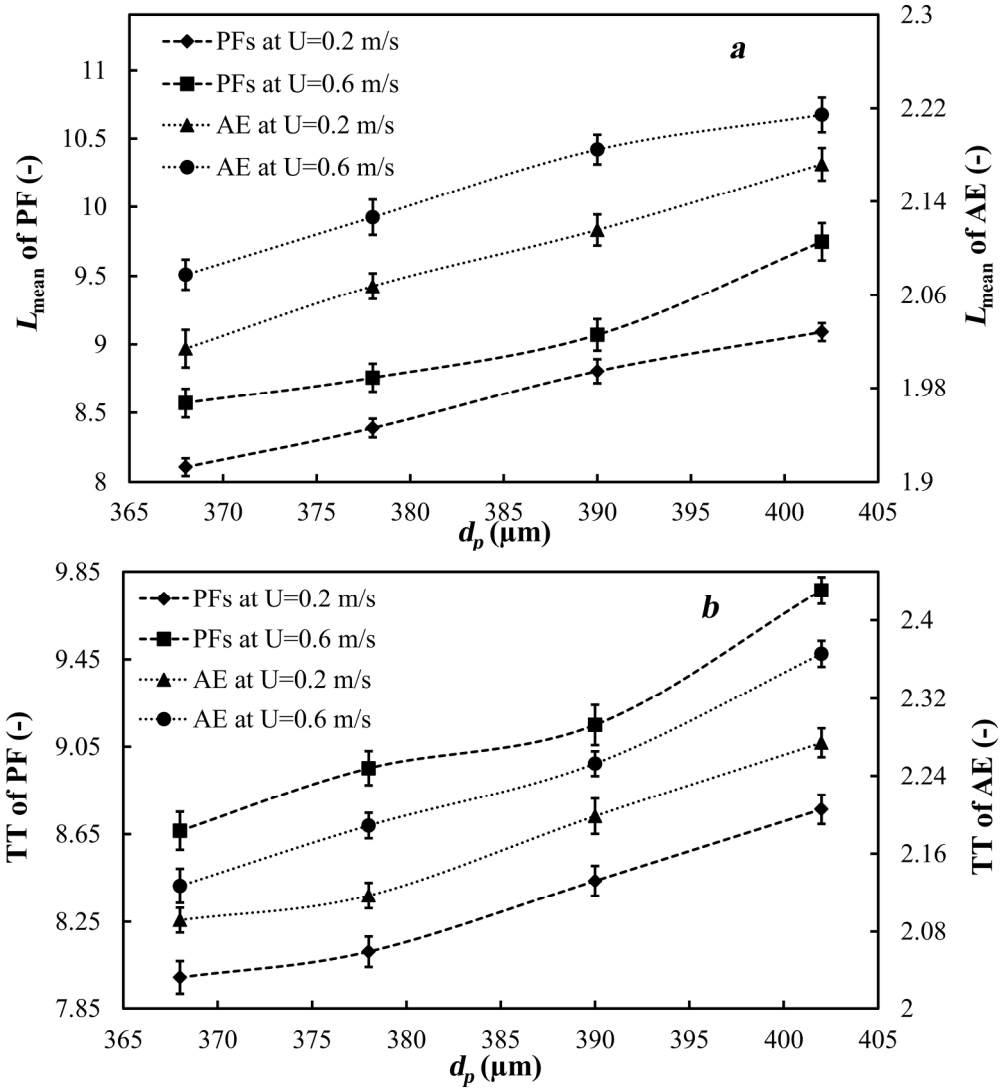

Figure 13. Average length of diagonal lines and trapping time versus average particle size for PFs and AE signal at m=1, τ=1, ε=0.05.
207x229mm (300 x 300 DPI)

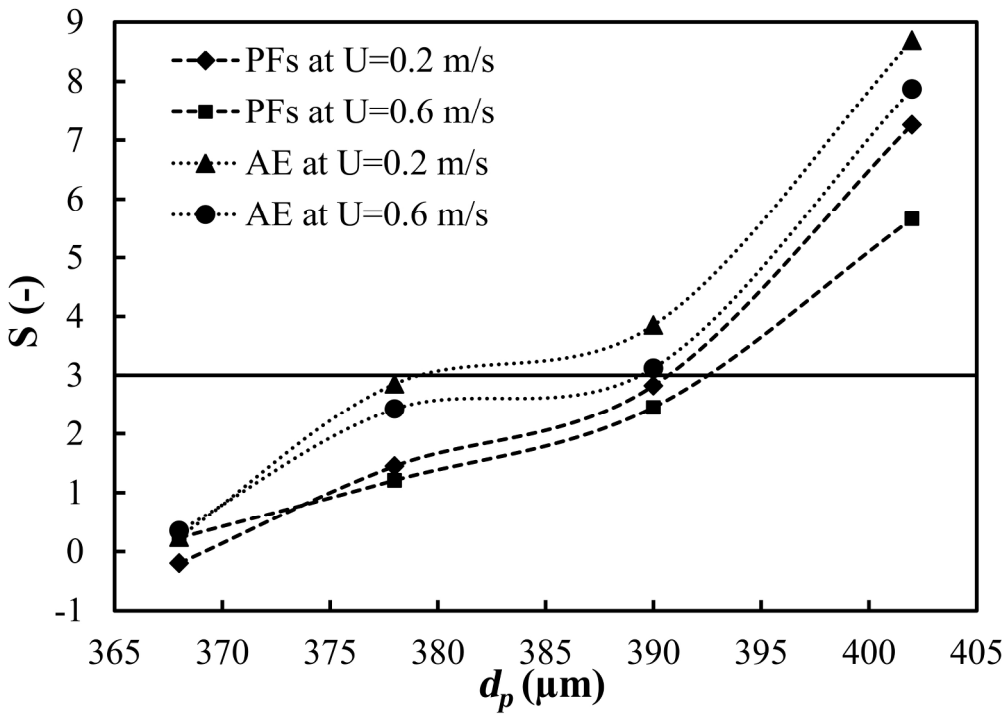

Figure 14. S-value versus average particle size for PFs and AE signal.
217x154mm (300 x 300 DPI)